Short Numerical Integrations of a Three-Level Spectral Quasi-Geostrophic Model

JULIA N. PAEGLE AND ALEXANDER E. MACDONALD

University of Utah, Salt Lake City, Utah 84112

(Manuscript received 9 November 1973; in revised form 28 June 1974)

ABSTRACT

Two sets of initial conditions are used to integrate a three-level quasi-geostrophic model in spectral form. After a maximum perturbation kinetic energy is reached, a barotropic exchange is established between the zonal flow and the perturbation with an apparent periodicity from 2 to 4 days. The initial state includes a finite amplitude baroclinic mode which is highly unstable in the linear sense. This mode exhibits a negative growth rate for about the first two days of the integration due to barotropic exchanges with other modes. Spectra of kinetic and available potential energies, enstrophy, and omega^2 are presented. The kinetic and available energy display a -3 slope for intermediate scales for the initial integration period when perturbation kinetic energy is actively growing at the expense of the mean flow available energy. The effect of the variation of stratification with height, dissipation, heating, mountains, and truncation of the spectral system is discussed.

1. Introduction

Observed spectral characteristics of atmospheric motions have been widely discussed in the literature (Deland, 1964; Eliasen and Machenhauer, 1965, 1969; Horn and Bryson, 1963; Kao and Wendell, 1970; Kao, Tsay, and Wendell, 1970; Kao, 1970; Kao, Jenne and Sagendorf, 1970; Mesinger, 1963; Murakami and Tomatsu, 1964; Saltzman and Peixoto, 1957; Saltzman and Fleischer, 1960, 1962; Saltzman and Tewels, 1964; Shapiro and Ward, 1960, 1963; Wiin-Nielsen, 1959, 1967; Wiin-Nielsen *et al.*, 1964; etc.).

In general, these observational works have shown that there is a maximum in the meridional kinetic energy spectra at about wavenumbers 5 to 7 in the atmosphere. The spectral distribution of kinetic energy with wavenumber seems to obey a simple power law of about -3 for wavenumbers larger than 8 to 10. Similar characteristics hold for the temperature spectra.

Wavenumbers 5 to 10 appear to give energy to lower and higher wavenumbers through nonlinear exchange processes, and resemble baroclinically unstable waves, deriving their kinetic energy from conversion of potential to kinetic energy. Almost all wavenumbers contribute to the kinetic energy of the mean zonal flow, which is a characteristic of barotropically stable waves. Wavenumber 2 seems to be an exception to this general behavior. Computations by Saltzman and Tewels (1964) and Saltzman and Fleischer (1960) indicate that this wave is characterized by a positive conversion from potential to kinetic energy and a transfer of kinetic energy to other wavenumbers.

These observed motions result from a superposition of many physical processes. To isolate the relative importance of the different effects, numerous analytic and numerical models have been discussed. Barotropic spectral vorticity equations have been integrated by Lorenz (1960), Baer (1964, 1970) and others. Various initial states were considered to study the reaction of the flow to different modes and how new modes were generated through nonlinear interactions. These studies give the general characteristics of wave to wave transfers, but preclude baroclinicity and vertical transfers. Nonlinear transfers are also emphasized in recent works for two-dimensional and three-dimensional quasi-geostrophic turbulence (Kraichnan, 1967; Leith, 1968; Batchelor, 1969; Charney, 1971). These studies predict a -3 power law for the energy spectra when certain assumptions are made. Such studies are important to assess the predictability of atmospheric motions (Lorenz, 1969) but do not investigate the cyclic behavior of the atmosphere. Linear studies of baroclinic instability have attempted to assess the preferred scale of motion in analytic studies (see, for example, Eady, 1949, and Pedlosky, 1963, 1964). Some extension to finite amplitude effects has been made by Phillips (1954), Arakawa (1960), Gambo (1966), and Pedlosky (1970, 1972). Each of these models the effect of a single growing mode on the basic zonal current. The mathematical methods may be valid for only relatively weak nonlinearities, and in their single mode treatments they have precluded the possibility of energy transfer to other modes. It is natural to inquire what reality the growth rates and index cycle

periodicities and amplitudes predicted by such approaches have in a more general model, and whether they even represent first order effects in the presence of exchange processes in a more complete spectrum.

Mountains and heating as forcing mechanisms for stationary disturbances have been discussed by Derome and Wiin-Nielsen (1971) and Murakami (1967). They also neglected nonlinear exchanges.

It can be seen from this review that a framework has been set by previous studies which enables interpretation of the disparate phenomena observed in the atmosphere. The goal of this paper is to determine to which extent the various processes can be isolated in a series of controlled experiments with a numerical model which is sufficiently general to include all of these effects simultaneously, but simple enough to permit ready interpretation of the results.

Section 2 discusses the model and Section 3 gives some spectral characteristics of the time integrations. Section 4 discusses the time behavior of kinetic and available energies and energy exchanges.

2. Numerical model

a. Mathematical formulation

In the pressure system of coordinates the quasi-geostrophic model is described by

$$\frac{\partial \zeta}{\partial t}+\mathbf{V}\cdot\nabla\zeta+\beta v=f_0\frac{\partial \omega}{\partial p}+\gamma\nabla^2\xi, \tag{1}$$

$$S(p)\nabla^2\omega+f_0^2\frac{\partial^2\omega}{\partial p^2}$$

$$=f_0\frac{\partial}{\partial p}(\mathbf{V}\cdot\nabla\zeta_a)-\nabla^2\left(\mathbf{V}\cdot\nabla\frac{\partial\phi}{\partial p}\right)-\frac{R}{c_p p}\nabla^2 H, \tag{2}$$

$$\zeta_a=\zeta+f;\quad \zeta=\frac{1}{f_0}\nabla^2\phi,$$

where

ϕ is the geopotential of a constant pressure surface

f_0 is the Coriolis parameter at a central latitude

$\mathbf{V}=\frac{1}{f_0}\mathbf{k}\times\nabla\phi$ is the geostrophic wind

H is a heating function

R is the gas constant

c_p is the specific heat at constant pressure

$\mathbf{i}, \mathbf{j}, \mathbf{k}$ are the unit vectors in the zonal, meridional and vertical directions, respectively

$S(p)=-\frac{\alpha}{\theta}\frac{\partial\theta}{\partial p}$ is the static stability

α is the specific volume

θ is the potential temperature

β is the beta parameter

$\nabla=\mathbf{i}\left.\frac{\partial}{\partial x}\right|_p+\mathbf{j}\left.\frac{\partial}{\partial y}\right|_p$ is the horizontal gradient operator

$\omega=\frac{dp}{dt}$ is the vertical velocity

$\gamma=80{,}000\frac{m^2}{s}$ is the dissipation coefficient

The importance of dissipation in determining the asymptotic behavior of finite-amplitude baroclinic waves has been discussed by Pedlosky (1970, 1972) and Newell (1972). It appears that in the absence of dissipation an oscillation of the mean flow and baroclinic wave is attained while for dissipative systems a steady state for the wave amplitude may be expected. The numerical integration of Steinberg (1973) with a higher order spectral system include lateral mixing, but exhibit the oscillatory characteristics predicted by the more simplified analytic model in the absence of dissipation.

We have also chosen to include only lateral dissipation in our study using a three-level quasi-geostrophic model. The main reason for introducing lateral diffusion is to prevent a false accumulation of wave amplitude in the shortest modes, resulting from the numerical integrations. This is equivalent to the dissipation implicitly included in some grid point models.

The chosen diffusivity value is consistent with the amount of dissipation typically present in the grid point model of Smagorinsky *et al.* (1965). It is also comparable to the dissipation implicit in the Lax-Wendroff and Matsuno differencing schemes which have been used in the NCAR and UCLA general circulation models, respectively. Recent results from quasi-geostrophic models which also include Ekman pumping and internal dissipation are reported by Barros and Wiin-Nielsen (1974).

In the absence of heating, mountains, and friction, quasi-geostrophic models conserve pseudo potential vorticity (Λ) on a horizontal trajectory, kinetic plus available potential energy, and pseudo enstrophy integrated over the whole domain ($\bar{K}+\bar{A}$ and $\bar{L}^2$, re-

spectively) where Λ, $\bar{K}$, $\bar{A}$, and $\bar{L}^2$ are defined as:

$$\Lambda=\xi+f_0\frac{\partial}{\partial p}\frac{1}{S(p)}\frac{\partial\phi}{\partial p},$$

$$\bar{K}=\frac{1}{2gf_0^2}\int_{p=0}^{p_0}\int_{x=0}^{L_x}\int_{y=0}^{L_y}(\mathbf{k}\times\nabla\phi)\cdot(\mathbf{k}\times\nabla\phi)dxdydp,$$

$$\bar{A}=\frac{1}{2g}\int_{p=0}^{p_0}\int_{x=0}^{L_x}\int_{y=0}^{L_y}\frac{1}{S(p)}\left(\frac{\partial\phi}{\partial p}\right)^2dxdydp,$$

$$\bar{L}^2=\frac{1}{2g}\int_{p=0}^{p_0}\int_{x=0}^{L_x}\int_{y=0}^{L_y}\left\{\xi+f_0\frac{\partial\phi}{\partial p}\left[\frac{1}{S(p)}\frac{\partial\phi}{\partial p}\right]\right\}^2dxdydp.$$

The validity of the finite difference methods is tested by checking the time behavior of the conserved quantities during the numerical integration.

b. Spectral representation

The integrations are carried for a rectangular region simulating a hemispheric belt between two fixed latitudes. Therefore, cyclic conditions were chosen for the east and west boundaries. For the northern and southern boundaries we have followed Phillips (1956) in selecting the condition $\phi=0$. These conditions define a closed domain for the geostrophic flow and thus the conservation properties previously discussed should hold for the interior region. It has been customary to further impose the condition that the zonally averaged meridional wind ($\bar{v}$), which is entirely non-geostrophic, should also vanish at the lateral boundaries, so that these boundaries represent rigid walls for all orders of the motion. Phillips (1954) has shown that this implies a constant zonally averaged zonal wind at the boundaries and it results in a 3-cell small meridiona, circulation when a baroclinic mode is consideredl similar to the observed 3-cell hemispheric meridional circulation.

We have imposed the lateral boundary condition $\partial\bar{v}/\partial y=0$ instead of $\bar{v}=0$. Since $\bar{v}$ contains only the ageostrophic (divergent) component of the meridional wind, this condition leaves the domain closed for the quasi-geostrophic model advections. Therefore, $\partial\bar{\omega}/\partial p=0$ and $\bar{\omega}=0$ at the lateral boundaries for homogeneous vertical boundary conditions on ω. The condition $\partial\bar{v}/\partial y=0$ leads to a meridional circulation composed of one central Ferrel cell and two half cells when an unstable baroclinic mode is considered. Thus, the relative importance of the Ferrel cell is greater with the condition $\partial\bar{v}/\partial y=0$ than with $\bar{v}=0$, consistent with observational evidence for middle latitudes. Therefore, the following double Fourier expansions were chosen:

$$\phi(x,y,p,t)=\sum_{m=-\infty}^{\infty}\sum_{n=1}^{\infty}\phi_{mn}(t,p)e^{ik_mx}\sin l_ny, \tag{3}$$

$$\omega(x,y,p,t)=\sum_{m=-\infty}^{\infty}\sum_{n=1}^{\infty}W_{mn}(t,p)e^{ik_mx}\sin l_ny, \tag{4}$$

where

$$i=\sqrt{-1}$$

$$k_m=\frac{2\pi m}{L_x},\text{ the zonal }(x)\text{ wavenumber}$$

$$l_n=\frac{\pi n}{L_y},\text{ the meridional }(y)\text{ wavenumber}$$

$$m=\ldots\ -1,\ 0,\ 1,\ \ldots$$

$$n=1,\ 2,\ 3,\ \ldots$$

$$\Phi_{-mn}=\Phi_{mn}{}^*,\text{ the complex conjugate.}$$

Substitution of (3) and (4) in (1) and (2) yields the spectral quasi-geostrophic equations

$$\frac{d\Phi_{mn}}{dt}=\frac{-i}{2f_0\mathbf{k}_m{}^2}\sum_{r=-x_{\max}}^{x_{\max}}\left[\sum_{s=1}^{n-1}\mathbf{k}_R{}^2(\mathbf{k}\cdot\mathbf{k}_m\times\mathbf{k}_R)\Phi_{rs}\Phi_{m-r,n-s}\right.$$

$$-\sum_{s=n+1}^{y_{\max}}\mathbf{k}_R{}^2(\mathbf{k}\cdot\mathbf{k}_m\times\mathbf{k}_R)\Phi_{rs}\Phi_{m-r,s-n}$$

$$\left.+\sum_{s=1}^{y_{\max}-n}\mathbf{k}_R{}^2(k_ml_s+k_rl_n)\Phi_{rs}\Phi_{m-r,n+s}\right]$$

$$+\frac{iBk_m\Phi_{mn}}{\mathbf{k}_m{}^2}-\frac{f_0{}^2}{\mathbf{k}_m{}^2}\frac{\partial W_{mn}}{\partial p}, \tag{5}$$

$$-S(p)\mathbf{k}_m{}^2W_{mn}+f_0{}^2\frac{\partial^2W_{mn}}{\partial p^2}=iBk_m\frac{\partial\Phi_{mn}}{\partial p}$$

$$\frac{-i}{2f_0}\sum_{r=-x_{\max}}^{x_{\max}}\left\{\sum_{s=1}^{n-1}(\mathbf{k}\cdot\mathbf{k}_m\times\mathbf{k}_R)\left[\mathbf{k}_R{}^2\frac{\partial}{\partial p}(\Phi_{rs}\Phi_{m-r,n-s})\right.\right.$$

$$\left.-\mathbf{k}_m{}^2\frac{\partial\Phi_{rs}}{\partial p}\Phi_{m-r,n-s}\right]-\sum_{s=n+1}^{y_{\max}}(\mathbf{k}\cdot\mathbf{k}_m\times\mathbf{k}_R)$$

$$\times\left[\mathbf{k}_R{}^2\frac{\partial}{\partial p}(\Phi_{rs}\Phi_{m-r,s-n})-\mathbf{k}_m{}^2\frac{\partial\Phi_{rs}}{\partial p}\Phi_{m-r,s-n}\right]$$

$$+\sum_{s=1}^{y_{\max}-n}(k_ml_s+k_rl_n)\left[\mathbf{k}_R{}^2\frac{\partial}{\partial p}(\Phi_{rs}\Phi_{m-r,n+s})\right.$$

$$\left.\left.-\mathbf{k}_m{}^2\frac{\partial\Phi_{rs}}{\partial p}\Phi_{m-r,s+n}\right]\right\}, \tag{6}$$

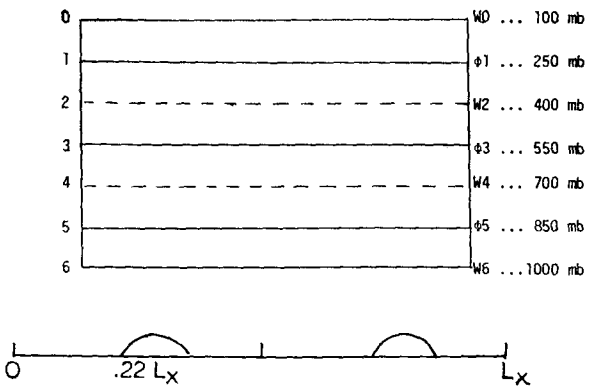

FIG. 1. The three-level model and mountain profile in the zonal direction.

where

$$\beta=\frac{\partial f}{\partial y}$$

$\mathbf{k}_m=k_m\mathbf{i}+l_n\mathbf{j}$, the wavenumber vector

$\mathbf{k}_m{}^2=\mathbf{k}_m\cdot\mathbf{k}_m$

r=dummy index for the x-direction wavenumber

s=dummy index for the y-direction wavenumber

The nonlinear terms are evaluated as convolutions in wavenumber space. Computational efficiency is achieved in the early stages of the integration by neglecting small terms in the nonlinear terms. For the chosen spectral resolution (25 modes in the zonal direction and 7 in the meridional direction) this method was considered to be about as efficient as that proposed by Orszag (1970). Furthermore, considerable reduction of computational effort is achieved if advantage is taken of the fact that states with initial energy constrained to even modes can only evolve into states which also have this characteristic.

TABLE I. Initial state for geopotential. The numbers are in m^2/s^2.

Case 1	Case 2	Level 1	Level 3	Level 5
$\phi_{4,1}$	$\phi_{3,1}$	500–800i	400–700i	−400i
$\phi_{2,1}$	$\phi_{1,2}/2$	200	170	100
$\phi_{0,2}$	$\phi_{0,2}$	2600	1400	560
$\phi_{8,4}$	$\phi_{6,4}$	400–600i	350–550i	−350i

c. Finite-difference model

The three-level model is presented in Fig. 1. Geopotentials are forecasted at levels 1, 3, and 5, while vertical velocities are obtained at levels 2, 4, and 6. The vertical boundary conditions $\omega_0=0$ and $\omega_6=0$ or ω_6 induced by mountains were chosen.

Two slightly different sets of initial geopotential values are considered. They are presented in Table 1 as Case 1 and Case 2. The complete initial states include also the conjugates of the given modes.

A high resolution run (50 modes in the zonal direction) is done with the initial conditions specified for

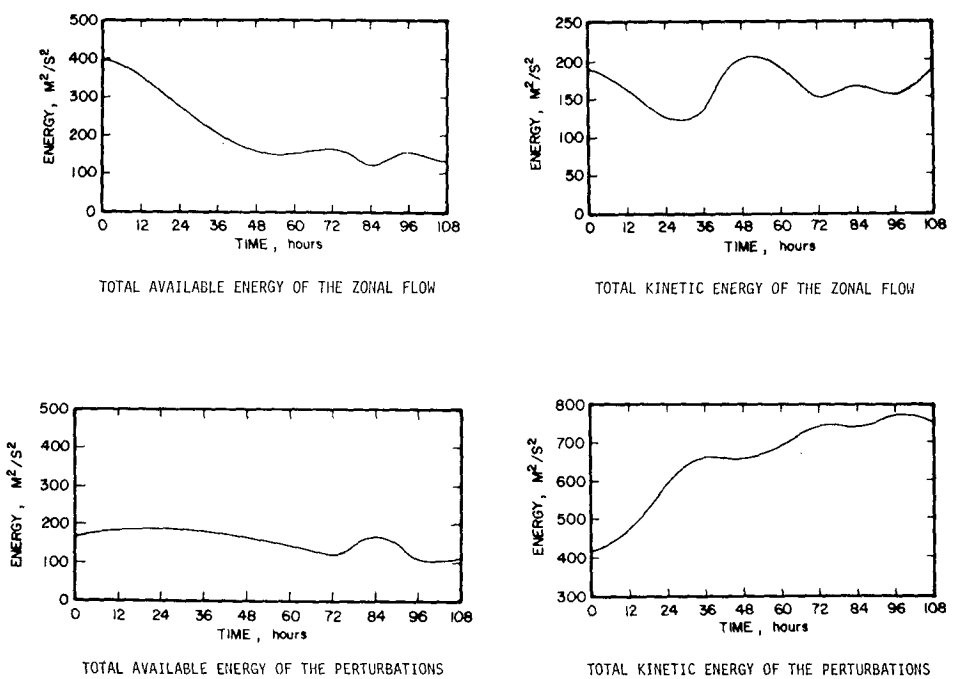

FIG. 2. Time series of available and kinetic energies for the perturbation and zonal flow for Case 1, run (a).

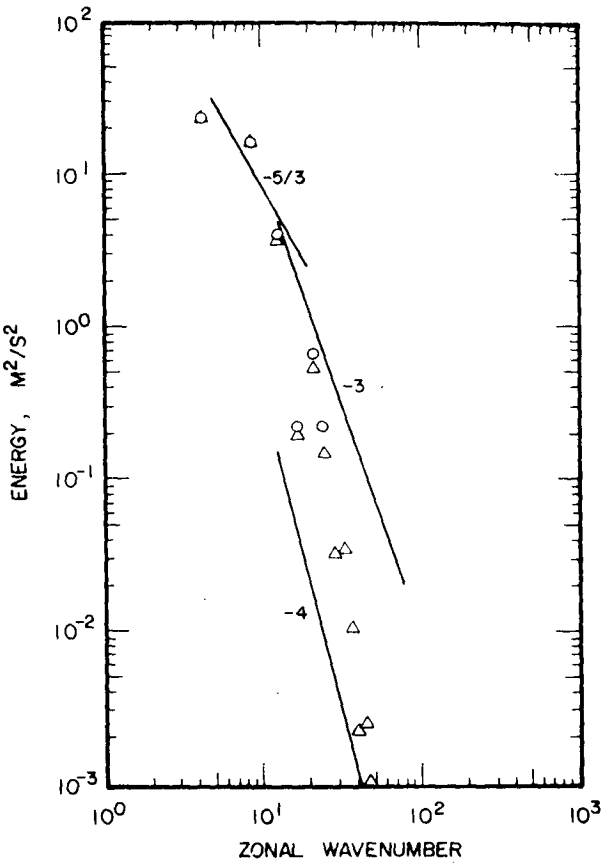

FIG. 3. The 850-mb kinetic energy as a function of zonal wavenumber for 24 hr for Case 1, 0-run (a), Δ-run (b).

Case 1, and thus the results from this case have been selected to emphasize the spectral characteristics of short waves.

For Case 2 a resolution of 25 zonal wavenumbers is considered. Here the emphasis shifts to longer waves and how they are influenced by different model parameters. The circulation is dominated by wavenumber 3 in low and high latitudes with a westerly jet in middle latitudes. The vertical shear of the zonal flow is such that linear baroclinic instability is expected.

We have followed Phillips (1956) in choosing a heating function independent of the motion. The Fourier coefficients h_{mn} for the heating function H in (2) are given in Table 2. The selected values are consistent with Brown's (1964) observations and are included at the lower level (700 mb).

A mountain effect is simulated through an imposed vertical velocity at level 6. It is included in mode number one in the meridional direction and in the zonal direction it is represented by the profile shown in Fig. 1. The Fourier decomposition in the zonal direction has a maximum at wavenumber 4, decaying as m^2 for longer wavenumbers.

TABLE 2. Selected heating function h_{mn}. The units are kJ/(ton·s).

$h_{02}=0.015$
$h_{22}=-0.0032-0.02i$

A meridionally independent zonal flow (henceforth referred to as mean zonal flow) is considered in certain cases. This flow has no vorticity and thus cannot be forecasted by the system of equations (1) and (2). The conservation of $\bar{A}+\bar{K}$ and $\bar{L}^2$ are used to obtain predictive equations for the meridionally independent thermal wind at levels 1, 3, and 5. This approach is similar to that used by Gambo (1966). The initial values used for the mean zonal flow are 25 m/s, 15 m/s, and 7 m/s at levels 1, 3, and 5, respectively. After a five-day integration without mean zonal flow or dissipation, it is found that energy is about 1.007 and pseudo-enstrophy 1.04 of the initial values.

Adams-Bashforth and leapfrog time differencing are both used in our integrations. Although the former scheme was suggested by both Lilly (1965) and Young (1968) for somewhat more highly truncated systems, the latter seemed to more closely conserve $\bar{A}+\bar{K}$ and $\bar{L}^2$ in our computations.

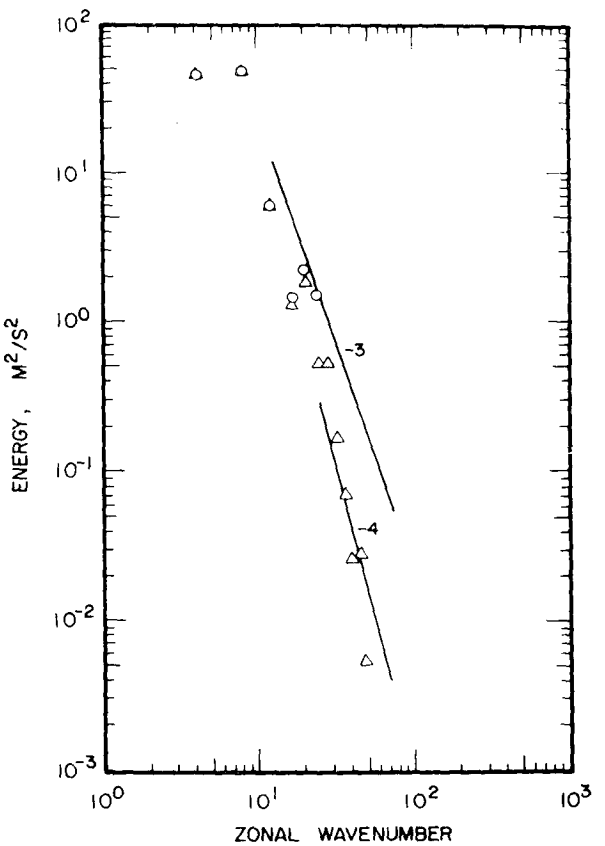

FIG. 4. The 550-mb kinetic energy as a function of zonal wavenumber for 24 hr for Case 1, 0-run (a), Δ-run (b).

3. Spectral characteristics

a. Case 1 results

The initial conditions presented in Table 1 for Case 1 are used in two runs [run (a) and run (b)]. Run (a) resolves up to 25 wavenumbers and run (b) up to 50 wavenumbers in the zonal direction. Both runs consider 7 wavenumbers in the meridional direction. Mean zonal winds, dissipation, heating and mountains are neglected in these runs. A static stability of 1.5×10^{-4} s^2 cm^4 gm^{-2}, consistent with Gates' (1961) observations, is used. Time series of perturbation and zonal energies for 4.5 days are presented in Fig. 2 for run (a). By then $\bar{A}+\bar{K}$ and $\bar{L}^2$ were 1.017 and 1.036 of their initial values, respectively. This figure shows that for the first 36 hr the perturbation kinetic energy increases while the available energy of the zonal flow decreases. After that the energy variations are similar to Steinberg's (1973) results for individual waves after about 10 days of integration. The maxima and minima of perturbation kinetic energy are in phase with the minima and maxima of kinetic energy of the zonal flow. This is consistent with Simons' (1972) analysis for an unstable baroclinic wave interacting with the zonal flow and a secondary wave. He has shown that, after an initial state in which the baroclinic wave grew, a barotropic stabilizing effect set in with an exchange of energy between the mean flow and the wave. Yang (1967) has also discussed the nonlinear effect for weakly unstable baroclinic waves. Steinberg (1973) and, more recently, Barros and Wiin-Nielsen (1974) have reported on the spectral characteristics of quasi-geostrophic flows after long time integrations, and compared them with Charney's (1971) predictions for quasi-geostrophic turbulence. The kinetic energy spectral slopes they obtained varied between -1.7 to -3.5 for zonal wavenumbers 7 to 20. For the available energy they report a -5 slope consistent with the vertical resolution of their models as discussed by Merilees and Warn (1972). It is of interest to compare their results with those we obtained during the initial period previously described. Figures 3 through 7 show the results for run (b) compared to those of run (a) at 24 hr. No computational instability is evident at this time.

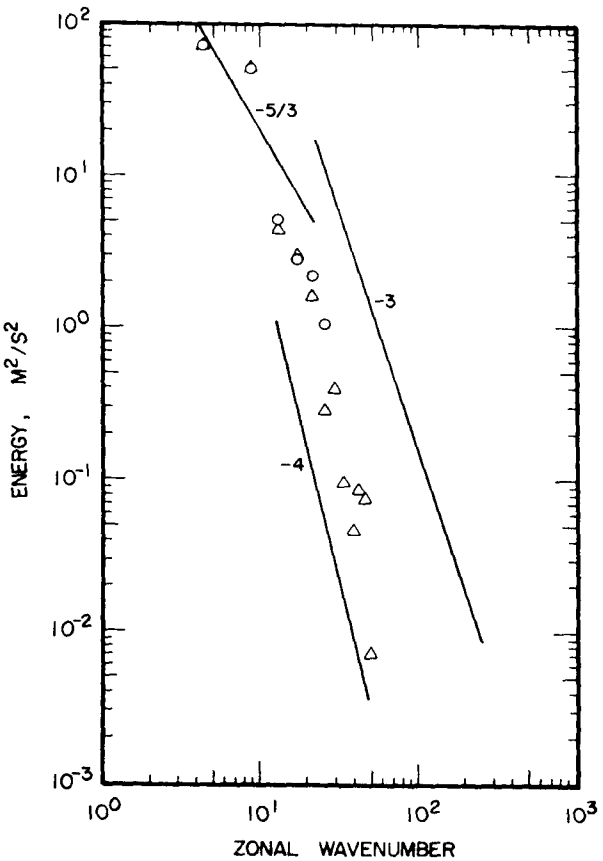

FIG. 5. The 250-mb kinetic energy as a function of zonal wavenumber for 24 hr for Case 1, 0-run (a), Δ-run (b).

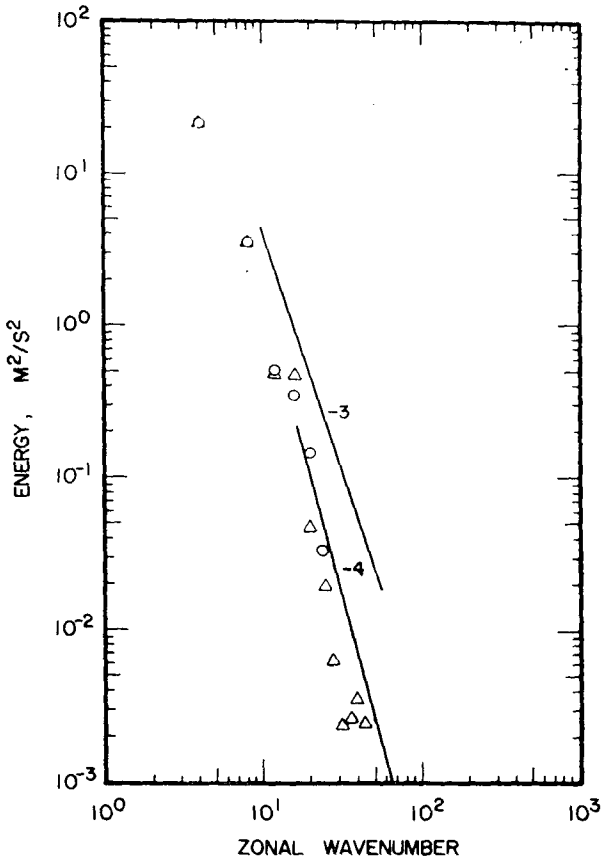

FIG. 6. The 400-mb available energy as a function of zonal wavenumber for 24 hr for Case 1, 0-run (a), Δ-run (b).

The energy spectra are quite similar for both the kinetic and available energies and indicate that three

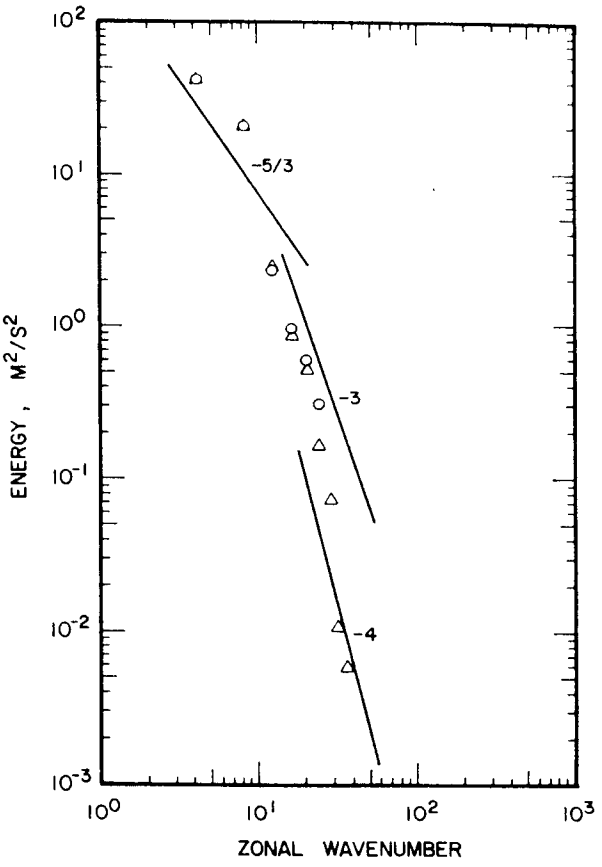

FIG. 7. The 700-mb available energy as a function of zonal wavenumber for 24 hr for Case 1, 0-run (a), Δ-run (b).

spectral regions can be delineated roughly as follows:

1) the $k^{-5/3}$ law holds quite crudely for wavenumbers smaller than 10;
2) the k^{-3} law holds quite well from wavenumbers 10 to 25;
3) at wavenumbers larger than 25 the slope is closer to a -4 than -3.

These results are similar to those obtained by Steinberg (1973) for the kinetic energy spectra, indicating that these spectral characteristics apply to various model formulations and at different stages of the integration. The available energy spectra at both levels at this time is qualitatively similar to that of the kinetic energy.

The effect of truncating the system is clearly seen in an excess energy at small waves for run (a) compared to run (b). A way to remove this excess energy is to introduce a dissipative effect as discussed previously. Thus the runs to be discussed next include a dissipation coefficient.

b. Case 2 results

The results presented in this section are obtained from the initial conditions for Case 2 presented in Table 1. Figures 8 through 10 present the kinetic energy, enstrophy, and omega² spectra vs. zonal wavenumber. A linear representation is now used to better isolate the long waves behavior. The quantities are summed over all meridional wavenumbers. The integration period is five days. Table 3 shows the modeling assumptions for each of the four depicted cases, which have been chosed to study the effect of vertically variable static stability, heat and mountains in the spectral model under study.

Figure 8 shows a relative maximum in the vicinity of wavenumber 3. As the system fluctuates, the long waves spectra change noticeably. For example, after 3 days of integration this relative maximum was shifted to wavenumber 6 (not shown). In general, the upper levels have more kinetic energy in the longer waves and less in the shorter waves than the lower levels. It is quite apparent from these experiments that topography and heating provide a major source of energy to all wavenumbers and not only to those of direct energy input. The enstrophy spectra (Fig. 9) show a distinct vertical variation in scale preference. At 850 mb (level 5) the enstrophy spectra are quite flat, with relative peaks of equal prominence, appearing in both long and short modes. The upper levels, however, are characterized by maxima at wavenumbers less than 7, with small contributions from shorter scales. This is not apparent in run (ii), characterized by equal stability at upper and lower levels.

The omega² spectra (Fig. 10) are similar to the lower level enstrophy spectra in that all scales seem to contribute markedly to the total power, except for some maxima between wavenumbers 6 and 20 for the different cases. Thus, if an observational system is designed for a certain acceptable error in these fields, the needed resolution would be much larger than when the energy is taken into account.

This might be clarified by considering the following classical argument (Charney, 1973, and others). Assume that the density spectrum of any quantity can be expressed as $E(k)=ck^{-\alpha}$ (where $\alpha>1$) for wavenumbers $k>k_c$. An observational system with maximum resolution given by k_0 is to be designed, in such a way that k_0 is as small as possible but satisfies the condition that

$$\int_{k_0}^{\infty} E(k)dk \Big/ \int_{k_c}^{\infty} E(k)dk = \frac{1}{\gamma}.$$

Here $1/\gamma^*$ 100 would represent the acceptable percentage error in this wavenumber region.

Thus

$$k_0^{-(\alpha-1)} = \frac{1}{\gamma} k_c^{-(\alpha-1)}$$

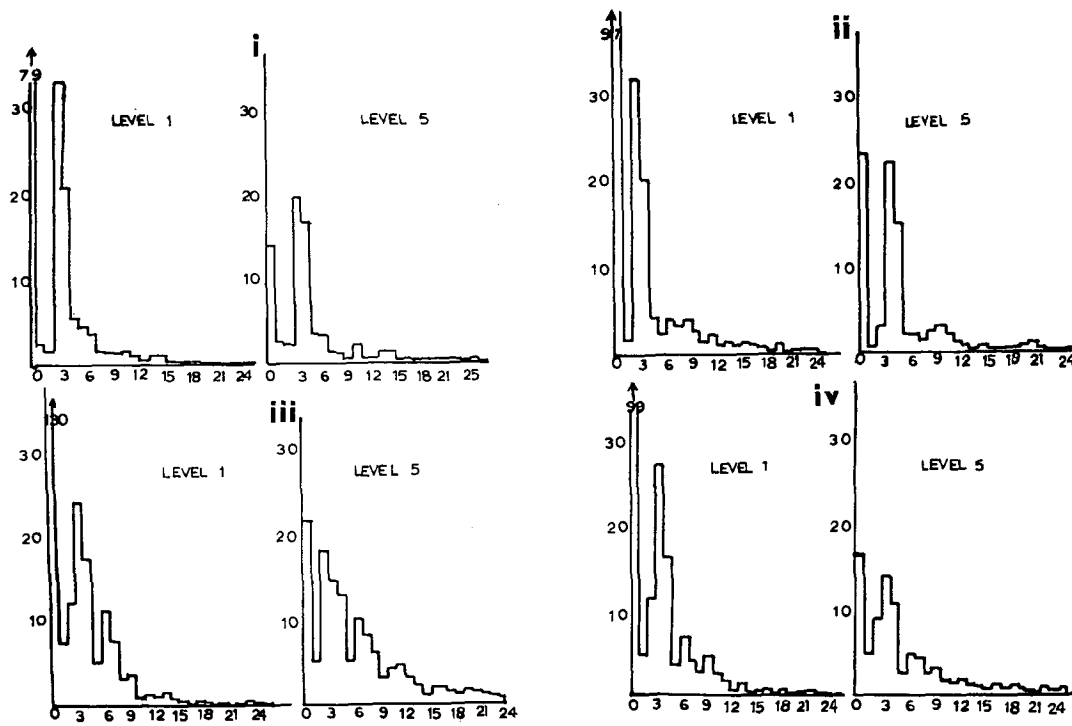

FIG. 8. Kinetic energy spectrum in $m^2 s^{-2}$ vs. zonal wavenumbers summed over all meridional modes for Case 2.

or

$$k_0 = \gamma^{1/(\alpha-1)} k_c.$$

Table 4 shows $\gamma^{1/(\alpha-1)}$ for different values of α and γ. The flatter the spectrum is, the higher the resolution needed. If the spectrum is fairly steep (i.e., α larger than 3), the error can be decreased from 20% to 5% with less than doubling the resolution.

The decrease of the amplitudes of the omega^2 spectra with height for runs (i), (iii), and to some

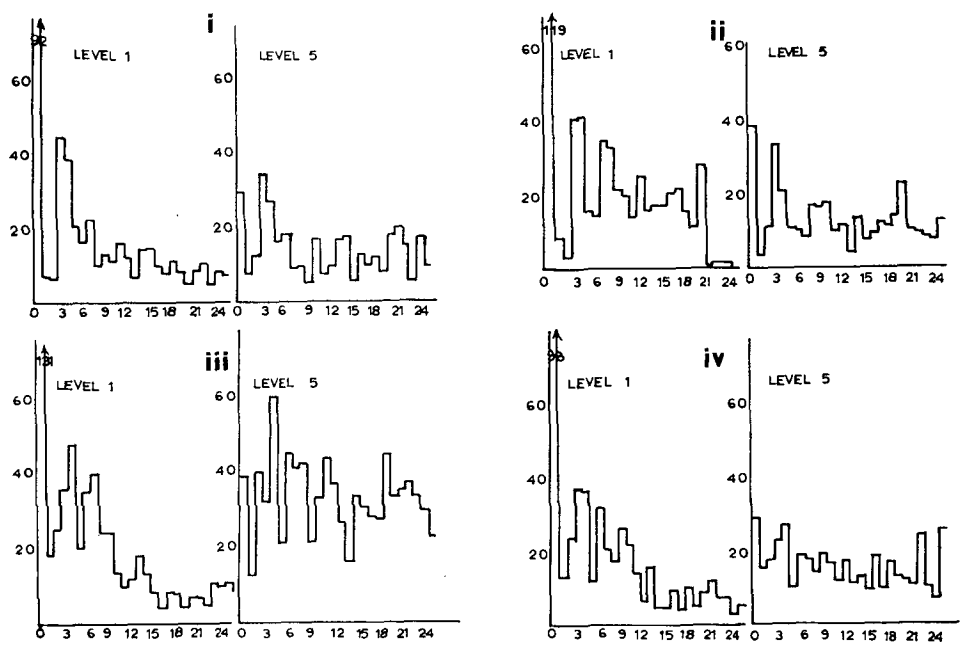

FIG. 9. Same as Fig. 8 but for enstrophy in $10^{-12} s^{-2}$.

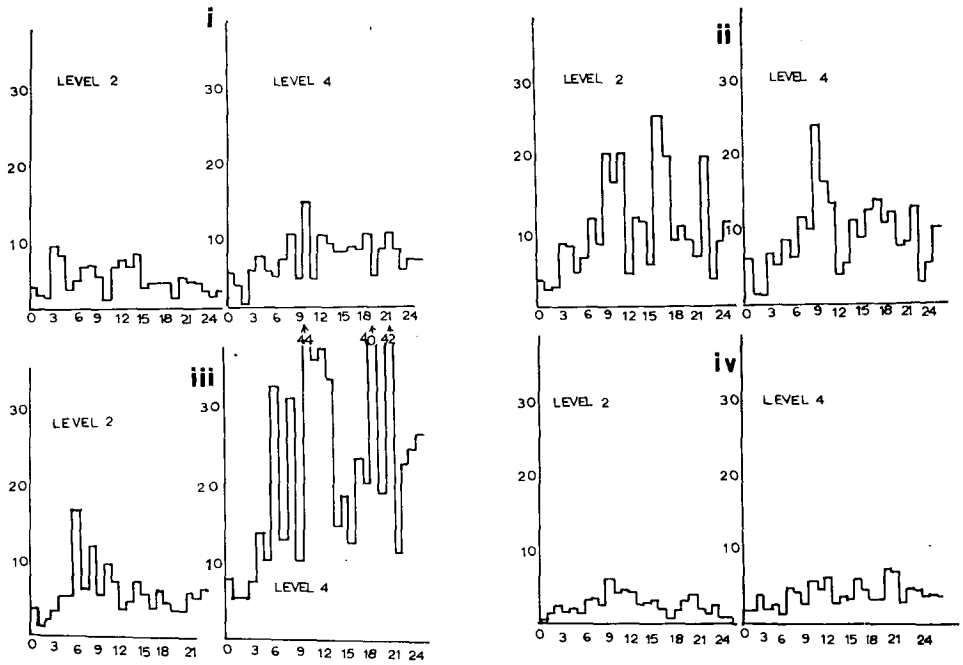

FIG. 10. Same as Fig. 8 but for omega^2 in 10^{-8} mb^2 s^{-2}.

extent (iv) is expected, since the upper layer is more stable than the lower layer for these runs.

4. Time evolution of kinetic and available energies

Figure 11 shows the energies for a zonal mode (0, 2) and a wave mode (3, 1) as a function of time for the four runs of Case 2 discussed in the last section. Together with mode (−3, 1) they form an interacting triad. This interaction is evident in the time behavior of their kinetic energies. The amplitude of the time oscillation is largest for run (ii) and increases with height. A decrease of zonal available energy is evident in most runs. The general characteristics of the baroclinic conversions can be obtained from Fig. 12, which depicts total kinetic and available energies at all levels. The conservation from available potential to kinetic energy is apparent up to about three days. From then on the time changes are quite small. Run (iii) differs quite markedly from the other runs in this aspect. The heating at the lower level results in a continuous source of kinetic energy. This effect is most pronounced at the lower level and is transferred vertically to the higher levels.

Figures 13 and 14 compare perturbation and zonal kinetic and available energies. The exchanges between zonal and perturbation kinetic energy resemble those described previously between modes (0, 2) and (3, 1). The decrease in the zonal available energy results in an increase of perturbation kinetic energy. The extra available energy at the upper level of run (ii) with respect to that of run (i) is transformed in a large extent into perturbation kinetic energy of the upper level. This baroclinic exchange tends to phase more closely the maximum of perturbation with the minimum of zonal kinetic energy.

The pronounced baroclinic conversions resulting from the heating in run (iii) are apparent in Figs. 13 and 14. The zonal available energy at 700 mb increases up to 3 days, decreasing from then on. This suggests that the transport of heat by the disturbances overcompensates the external zonal heatings after 3 days. From then on the perturbation kinetic energies increase steadily in run (iii). The behavior of the other runs is quite different.

TABLE 3. Modeling assumptions for runs (i), (ii), (iii), and (iv).

	(i)	(ii)	(iii)	(iv)
$S_2(\times 10^{-4}$ s^2 cm^4 gm$^{-2})$	3.0	1.5	3.0	3.0
$S_4(\times 10^{-4}$ s^2 cm^4 gm$^{-4})$	1.5	1.5	1.5	1.5
Mean zonal wind	x	x		
Sensible heat			x	
Topography				x

TABLE 4. $\gamma^{1/(\alpha-1)}$ for different values of α and γ.

α \ γ	5	10	20
4/3	125	1000	8000
5/3	11.2	32	796
2	5	10	20
2.5	2.9	4.6	7.4
3	2.2	3.2	4.5
4	1.7	2.15	2.7
5	1.5	1.8	2.1

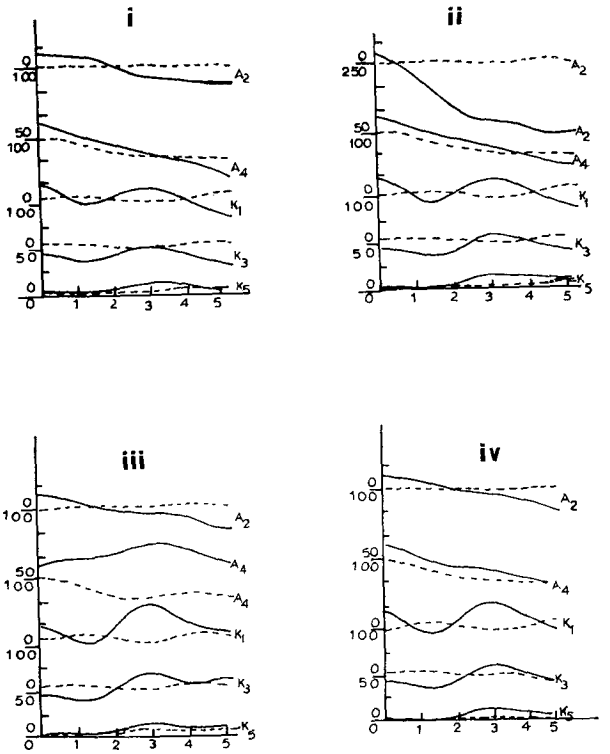

FIG. 11. Available energies at 400 mb (A_2) and 700 mb (A_4) and kinetic energies at 250 mb (K_1), 550 mb (K_3), and 850 mb (K_5) for zonal mode (0, 2) (solid line) and wave mode (3, 1) (dashed line) vs. time in days. In the ordinate the upper and lower scale indicate the origin for the wave and zonal mode, respectively.

For all runs it is evident that, although an increase of total perturbation kinetic energy appears, this increase is not present in the most unstable baroclinic modes. This is particularly evident for the (6, 4) mode,

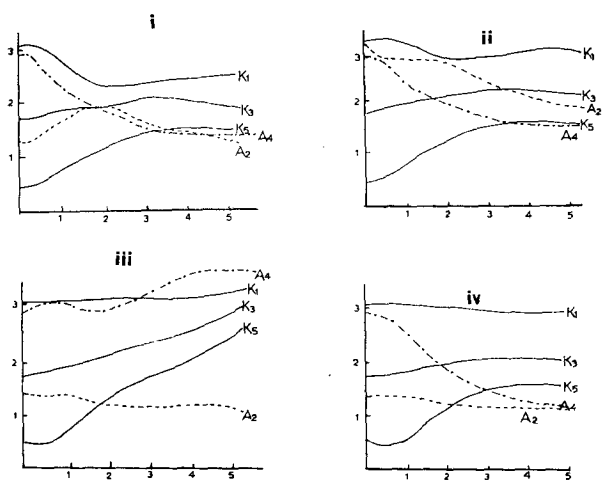

FIG. 12. Kinetic energies (solid lines) at 250 mb (K_1), 500 mb (K_3), and 850 mb (K_5) and available energies at 400 mb (A_2) (dashed line) and 700 mb (A_4) (dash-dotted line) vs. time in days. The ordinate is in units of 100 m^2 s^{-2}.

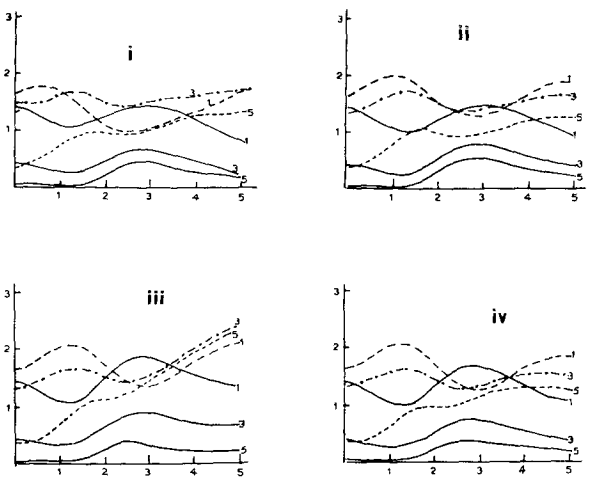

FIG. 13. Total zonal (solid lines) and perturbation (dashed and dash-dotted lines) kinetic energies at 250 mb (1), 550 mb (3) and 850 mb (5) vs. time in days. The ordinates are in units of 100 m^2 s^{-2}.

which is highly unstable in the linear sense. The chosen initial state describes a westerly tilt of this wave with height for the lower half of the atmosphere so that baroclinic development is expected. Nevertheless, this mode loses most of its initial kinetic energy in 2 days. Thus it is apparent that the linear baroclinic instability concepts may not be adequate to describe the energy behavior when barotropic effects are present, as pointed out by Simons (1972) and Yang (1967) for much lower spectral systems.

5. Summary and conclusions

A three-level quasi-geostrophic spectral model was integrated for about 5 days to simulate atmospheric

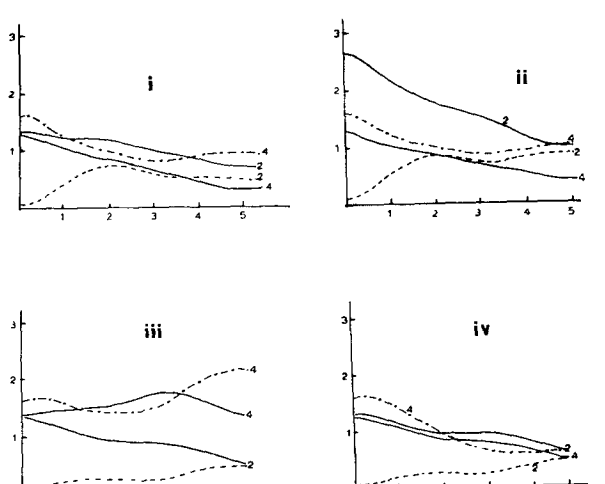

FIG. 14. Total zonal (solid lines) and perturbation (dashed and dash-dotted lines) available energy at 400 mb (2) and 700 mb (4) vs. time in days. Ordinate units are 100 m^2 s^{-2}.

processes in a latitudinal belt centered at middle latitudes. Different runs were made to study the effects of dissipation, truncation of the spectral system, mountains, heating, and vertically variable static stability upon the spectral characteristics of the atmosphere and in the time behavior of different energy forms.

The three-level model allows more realistic study of the low-level baroclinic developments, which are often missed by two-level models, as pointed out by Charney (1954). Lateral boundary conditions are introduced to define a closed domain for the quasi-geostrophic waves but open for the meridional circulation. These boundary conditions are proposed as a more realistic simulation of flows at middle latitudes when only a latitudinal belt and not the whole hemisphere is considered.

The principal findings of this article can be summarized as follows:

1) The kinetic energy of the perturbation initially increases at the expense of the available energy of the zonal flow. After a maximum perturbation kinetic energy is reached, a barotropic exchange is established between the zonal flow and the perturbations with an apparent periodicity from 2 to 4 days (Figs. 2, 11, 13). This is consistent with Simons' (1972) analysis of a baroclinically unstable wave interacting with the zonal flow and a secondary wave.
2) Even in the initial state of perturbation kinetic energy increase discussed above, no preferred growth was observed in the modes predicted by linear theory. Negative growth rate for the first 36 hr was observed for the finite amplitude unstable baroclinic wave initially present.
3) The spectra of kinetic and available energy show a very large contribution from long waves. The power laws which describe the dependence of the energy spectra with the higher wavenumbers are quite sensitive to the resolution of the system and the assumed dissipation.
4) For the initial baroclinic stage the following spectral slopes were found for the kinetic and available energy: from zonal wavenumbers 1–10, a $-5/3$ slope; from 10–25, a -3 slope, and from 25–50, a -4 slope. These slopes are similar to those obtained for the kinetic energy spectra by Steinberg (1973) and Barros and Wiin-Nielsen (1974), after considerably longer integration periods.
5) The spectra of enstrophy and omega^2 are much flatter than the energy spectra, as exptected from the functional dependence of these quantities on the geopotential fields. Thus, if it is desired to base an observational system in terms of these fields, the resolution required would be considerably larger than when the energy is considered.
6) The spectral decomposition clearly indicates the trapping of short waves in the lower layers as a consequence of the variation of the stratification with height.

The conclusions of this study may depend to a certain extent on model limitations. A primitive equation model on a sphere would remove the limitation of quasi-geostrophic flow semi-bounded on a rectangular region, and would approximate the atmosphere more closely. Future work may emphasize better vertical resolution and more realistic heating and dissipation processes.

Acknowledgments. The authors wish to express their gratitude to Professors S-K Kao and J. Paegle for their encouragement and helpful discussions. This work has been supported by the National Science Foundation under Grant GA-29200.

REFERENCES

Arakawa, A., 1960: Non-geostrophic effects in the baroclinic prognostic equations. *Proc. Internat. Symposium Numerical Weather Prediction*, Tokyo, 161–175.

Baer, F., 1964: Integration with the spectral vorticity equation. *J. Atmos. Sci.*, **21**, 260–276.

——, 1970: Dependence on the highly truncated spectral vorticity equation on initial conditions. *J. Atmos. Sci.*, **27**, 987–999.

Barros, V. R., and A. Wiin-Nielsen, 1974: On quasi-geostrophic turbulence: a numerical experiment. *J. Atmos. Sci.*, **31**, 609–621.

Batchelor, G. K., 1969: Computations of the energy spectrum in homogeneous two-dimensional turbulence. *Phys. Fluids Suppl. II*, **12**, 233–239.

Brown, J. A., 1964: A diagnostic study of tropospheric diabatic heating and the generation of available potential energy. *Tellus*, **16**, 371–388.

Charney, J. G., 1954: Numerical prediction of cyclogenesis. *Proc. Natl. Acad. Sci.*, **40**, 99–110.

——, 1971: Geostrophic turbulence. *J. Atmos. Sci.*, **28**, 1087–1095.

——, 1973: Geostrophic turbulence. Paper presented at second Conference on Numerical Weather Prediction of the Amer. Meteor. Soc., Monterey. Abstract in *Bu.. Amer. Meteor. Soc.*, **54**, p. 740.

Deland, R. J., 1964: Traveling planetary waves. *Tellus*, **16**, 271–273.

Derome, J., and A. Wiin-Nielsen, 1971: The response of a middle-latitude model atmosphere to forcing by topography and stationary heat sources. *Mon. Wea. Rev.*, **99**, 564–576.

Eady, E. T., 1949: Long waves and cyclone waves. *Tellus*, **1**, 33–52.

Eliasen, E., and B. Machenhauer, 1965: A study of the fluctuations of the atmospheric planetary patterns represented by spherical harmonics. *Tellus*, **17**, 220–238.

——, 1969: Large scale atmospheric wave motions. *Tellus*, **21**, 149–165.

Gambo, K., 1966: Some remarks on the treatment of finite amplitude disturbances in the baroclinic atmosphere. *J. Meteor. Soc. Japan*, **44**, 109–121.

Gates, W. L., 1961: Static stability measures in the atmosphere. *J. of Met.* **18**, 526–533.

Horn, L. H., and R. A. Bryson, 1963: An analysis of the geostrophic kinetic energy spectrum of large-scale atmospheric turbulence. *J. Geophys. Res.*, **68**, 4, 1059–1064.

Kao, S.-K., 1970: Wavenumber-frequency spectra of temperature in the free atmosphere. *J. Atmos. Sci.*, **27**, 1000–1007.

——, R. L. Jenne, and J. F. Sagendorf, 1970: The kinetic energy of large scale atmospheric motion in wavenumber frequency space: I. Mid-troposphere of the Southern Hemisphere. *J. Atmos. Sci.*, **27**, 1008–1020.

——, C.-Y. Tsay, and L. L. Wendell, 1970: The meridional transport of angular momentum in wavenumber-frequency space. *J. Atmos. Sci.*, **27**, 614–626.

——, and L. L. Wendell, 1970: The kinetic energy of the large scale atmospheric motion in wavenumber-frequency space. *J. Atmos. Sci.*, **27**, 359–375.

Kraichnan, R. H., 1967: Inertial ranges in two dimensional turbulence. *Phys. Fluids*, **10**, 1417–1423.

Leith, C. E., 1968: Diffusion approximation for two dimensional turbulence. *Phys. Fluids*, **11**, 671–672.

Lilly, D. K., 1965: On the computational stability of numerical solutions of time-dependent nonlinear geophysical fluid dynamic problems. *Mon. Wea. Rev.*, **93**, 11–26.

Lorenz, E. N., 1960: Maximum simplification of the dynamic equations. *Tellus*, **12**, 243–254.

——, 1969: The predictability of a flow which possesses many scales of motion. *Tellus*, **21**, 289–307.

Merilees, P. E., and T. Warn, 1972: The resolution implications of geostrophic turbulence. *J. Atmos. Sci.*, **29**, 990–991.

Mesinger, F., 1963: On the two-dimensional spectral analysis of kinetic energy over a circumpolar area of a sphere. Darmstadt, Tech. Note N.S., Contract AF 61(052), AFCRL 64-248.

Murakami, T., 1967: Vertical transfer of energy due to stationary disturbances induced by topography and diabatic heat sources and sinks. *J. Meteor. Soc. Japan*, **45**, 205–230.

——, and K. Tomatsu, 1964: The spectrum analysis of the energy interaction terms in the atmosphere. *J. Meteor. Soc. Japan*, **42**, 14–25.

Newell, A. C., 1972: The post bifurcation stage of baroclinic instability. *J. Atmos. Sci.*, **29**, 64–76.

Orszag, S. A., 1970: Transform method for the calculation of vector-coupled sums: Application to the spectral form of the vorticity equation. *J. Atmos. Sci.*, **27**, 890–894.

Pedlosky, J., 1963: Baroclinic instability in two-layer systems. *Tellus*, **15**, 20–25.

——, 1964: The stability of currents in the atmosphere and the ocean. *J. Atmos. Sci.*, **21**, 201–219, 342–353.

——, 1970: Finite-amplitude baroclinic waves. *J. Atmos. Sci.*, **28**, 145–161.

——, 1972: Limit cycles and unstable baroclinic waves. *J. Atmos. Sci.*, **29**, 53–63.

Phillips, N. A., 1954: Energy transformations and meridional circulations associated with simple baroclinic waves in a two-level, quasi-geostrophic model. *Tellus*, **6**, 273–286.

——, 1956: The general circulation of the atmosphere: a numerical experiment. *Quart. J. Roy. Meteor. Soc.*, **82**, 123–164.

Saltzman, B., and A. Fleisher, 1960: The modes of release of available potential energy in the atmosphere. *J. Geophys. Res.*, **65**, 1215–1222.

——, and ——, 1962: Spectral statistics of the wind at 500 mb. *J. Atmos. Sci.*, **19**, 195–204.

——, and J. P. Peixoto, 1957: Harmonic analysis of the mean northern hemisphere wind field for the year 1950. *Quart. J. Roy. Meteor. Soc.*, **83**, 360–364.

——, and S. Teweles, 1964: Further statistics on exchange between harmonic components of the atmospheric flow. *Tellus*, **16**, 432–435.

Shapiro, R., and F. Ward, 1960: The time-space spectrum of the geostrophic meridional kinetic energy. *J. Meteor.*, **17**, 621–626.

——, and ——, 1963: The kinetic energy spectrum of meridional flow in the mid-troposphere. *J. Atmos. Sci.*, **20**, 353–358.

Simons, T. J., 1972: The nonlinear dynamics of cyclone waves. *J. Atmos. Sci.*, **29**, 38–51.

Smagorinsky, J., S. Manabe, and J. L. Holloway, 1965: Numerical results from a nine-level general circulation model of the atmosphere. *Mon. Wea. Rev.*, **93**, 727–768.

Steinberg, H. L., 1973: Numerical simulation of quasi-geostrophic turbulence. *Tellus*, **25**, 233–246.

Wiin-Nielsen, A., 1959: A study of energy conversions and meridional circulation for the large scale motion in the atmosphere. *Mon. Wea. Rev.*, **87**, 319–332.

——, 1967: On the annual variation and spectral distribution of atmospheric energy. *Tellus*, **19**, 540–559.

——, J. A. Brown, and M. Drake, 1964: Further studies of energy exchange between the zonal flow and the eddies. *Tellus*, **16**, 168–180.

Yang, Ch-H., 1967: Nonlinear aspects of the large scale motion in the atmosphere. Tech. Rept. 08759-1-T, The University of Michigan, Ann Arbor, 173 pp.

Young, J. A., 1968: Comparative properties of some time differencing schemes for linear and nonlinear oscillations. *Mon. Wea. Rev.*, **96**, 357–364.